Rational Amphiphilic Ligand Engineering Enables Enhanced Stability and Efficiency of CsPbBr$_3$ Nanocrystals Based Light Emitting Diodes

Yanyan Duan, Kalyani Chordiya, Mousumi Upadhyay Kahaly, Freddy E. Oropeza, Víctor A. de la Peña O'Shea, De-Yi Wang,* and Rubén D. Costa*

Metal halide perovskites have shown great potential for lighting. However, their low stability under irradiation/thermal stress and/or ambient storage conditions are critical for light-emitting diodes (LEDs). Among the stabilization strategies, ligand surface modification is effective toward stable perovskites, but the dynamic ligand adsorption/desorption process on the surface is a limiting factor. Herein, a new family of biogenic and amphiphilic capping agents, phosphatidyl-L-serine (Ptd-L-Ser), combining stronger multibinding motifs compared to conventional capping agents has led to superior CsPbBr$_3$ (CsPbBr$_3$-Ptd-L-Ser) with significantly enhanced stability upon storage/heating/water, keeping excellent photoluminescence quantum yields of ≈80% over half year. Spectroscopic/theoretical studies reveal that the origin of this behavior is the increased exciton binding energy associated to the versatility of multiple bindings. This results in CsPbBr$_3$-Ptd-L-Ser nanocrystals-based green-LEDs featuring excellent stabilities of >700 h (20 mA) and >200 h (100 mA) that strongly contrast with the reference devices with pristine CsPbBr$_3$ nanocrystals (120 h (20 mA) and 27 h (100 mA)). White LEDs (WLEDs) with chromaticity coordinates of (0.34, 0.33) and high luminous efficiency of 76 lm W^{-1}, keeping stable over weeks, are further demonstrated under continuous operational conditions, thereby suggesting CsPbBr$_3$-Ptd-L-Ser nanocrystals can be a potential candidate for commercial WLED technology.

1. Introduction

In the last decade, metal halide perovskites (MHPs) with a well-known structure of ABX$_3$ (where A is the monovalent cation,

B is the bivalent cation, and X is the halide anion) have become an emerging class of materials in photonics, optoelectronics, and catalysis, among others.[1–5] Here, the all-inorganic cesium lead halide perovskites are emerging materials for phosphor-converted light-emitting diodes (pc-LEDs).[6–8] This is largely motivated by their unique chemical and optical characteristics, such as defect-tolerance,[9] narrow full width at half-maximum (FWHM),[10] easy tunable emission spectra,[6] excellent photoluminescence quantum yields (PLQYs, as high as >80%),[11] as well as easy processability,[12] among others. However, their notorious poor stability has hindered further technological developments. In short, they are prone to decomposition and/or aggregation under ambient (moisture and oxygen) storage conditions, irradiation/thermal stress, and device fabrication and operational conditions.[13–15] The preparation of MHPs has been realized following the conventional hot-injection or ligand-assisted reprecipitation methods, in which oleylamine (OLA) and oleic acid (OA) are usually selected as the ligands to increase the solubility of MHPs' precursors and to control MHPs' size.[6,12,16] The highly dynamic ligand bonding between the MHPs core and the above capping ligands always results

Y. Duan, D.-Y. Wang
IMDEA Materials Institute
Calle Eric Kandel 2, Getafe 28906, Spain
E-mail: deyi.wang@imdea.org
K. Chordiya, M. U. Kahaly
ELI ALPS
ELI-HU Non-Profit Ltd
Wolfgang Sandner utca 3, Szeged H-6728, Hungary

The ORCID identification number(s) for the author(s) of this article can be found under https://doi.org/10.1002/adom.202201176.

K. Chordiya, M. U. Kahaly
Institute of Physics
University of Szeged
Dóm tér 9, Szeged H-6720, Hungary
F. E. Oropeza, V. A. de la Peña O'Shea
Photoactivated Processes Unit
IMDEA Energy Institute
Avda. Ramón de la Sagra, 3, Mostoles, Madrid 28935, Spain
R. D. Costa
Chair of Biogenic Functional Materials
Technical University of Munich
Schulgasse 22, D-94315 Straubing, Germany
E-mail: ruben.costa@tum.de

in a weak coordination.[17] Indeed, they tend to decoordinate from the surface of the MHPs upon isolation and purification, reducing both, PLQYs and stabilities, as the number of surface trap states is increased as well as aggregation and/or phase transitions are promoted.[18,19]

In this context, several strategies have been developed to improve the colloidal stability of MHPs, such as encapsulation with metal oxides[8,10,20] or metal–organic frameworks (MOFs)[21–23] through physical mixing/chemical process, embedding the MHPs inside the hydrophobic polymers via in situ and ex situ methods.[15,24] Metal oxide and polymer shells provide a barrier for moisture and oxygen, improving MHPs' resistance against irradiation and thermal stress. However, MHPs usually aggregate upon polymer composite forming, while the insulation feature of the widely used transparent metal oxide (e.g., SiO_2) limits their application in optoelectronics.

As an alternative method, ligand engineering, including using zwitterionic or amphiphilic compounds, has been barely explored to enhance MHPs' stability as well as retain their size and shape. The benefits of this approach are: i) strong electronic coupling via chelating and selective ligands (e.g., 2,2'-iminodibenzoic acid,[25] poly(maleic anhydride-alt-1-octadecene),[26] lecithin,[27] poly(methyl methacrylate)-block-poly(tert-butylacrylate),[28] etc.), ii) surface curing of defects and/or vacancies (e.g., ethylenediaminetetraacetic acid and glutathione are postulated to "strip" the undercoordinated Pb from the $MAPb(I_xBr_{1-x})_3$, leading to smaller sizes, enhanced PLQYs as well as reduced phase segregation),[2] and iii) large steric hindrance as well as resistance against the environmental stress (e.g., poly(acrylic acid)-*block*-polystyrene (PAA-*b*-PS), in which carboxyl groups of inner PAA blocks strongly bind to the surface, while the outer hydrophobic PS chains form a shell surrounding around the $CsPbBr_3$).[29]

Along these lines, this work shows how a new family of biogenic representatives phosphatidyl-L-serine (Ptd-L-Ser) leads to superior ligand@$CsPbBr_3$ compounds compared to the above prior-art. Ptd-L-Ser is a well-known phospholipid component for the cell membranes that provides i) a large versatility for multiple binding motifs to strongly attach to the surface of $CsPbBr_3$ nanocrystals (NCs) and isolate undercoordinated ions without causing any crystalline deformation and ii) long hydrophobic chains as effective protecting shells. Indeed, the $CsPbBr_3$-Ptd-L-Ser features significantly improved PLQYs going from 30% to 90% and thermal stabilities due to the increased exciton binding energy (E_b) from ≈337 to 507 meV for OA/OLA and Ptd-L-Ser-capped $CsPbBr_3$ NCs, respectively. This is supported by simulations using density functional theory (DFT) to calculate the adsorption energy and electronic structure to estimate the stability and the change in bandgap with and without the incorporation of Ptd-L-Ser, respectively. DFT-based bonding analysis reveals that adsorption of Ptd-L-Ser is possible through multiple sites, which contrasts to the adsorption of OLA and OA ligands, that only happens through a single site. Indeed, the incorporation of Ptd-L-Ser ligands can stabilize the $CsPbBr_3$ through multiple possible allowed bonding sites as well as stronger bonds at the adsorption sites. This resulted in pc-LEDs with a high luminous efficiency of ≈70 lm W^{-1} and excellent operational stabilities of > 700 h (20 mA) and >200 h (100 mA), representing almost sevenfold enhancement compared to

reference devices with the pristine $CsPbBr_3$ NCs (45 lm W^{-1}; 120 and 27 h under 20 and 100 mA, respectively) as well as the prior-art ligand@$CsPbBr_3$ device (average 50 lm W^{-1} and stabilities of <200 h under 20 mA). Demonstration of such merits supports the successful fabrication of the white LEDs (WLEDs) with exciting performances, for example keeping in the white emission area over weeks with high luminous efficiency of more than 75 lm W^{-1}. In light of our findings, this work sets a new family of biogenic and amphiphilic capping ligands to stabilize $CsPbBr_3$ NCs that represents a significant advance toward sustainable perovskite-based lighting sources.

2. Results and Discussion

2.1. Synthesis, Characterizations, and Simulations

The pristine $CsPbBr_3$ NCs were prepared using the previous method with minor modifications.[6] The prepared Cs–oleate solution was quickly injected into the mixture of $PbBr_2$ and 1-octadecene (ODE) under 165 °C. The solution was moved to the ice-bath to quench the growth of the NCs after 5 s. The $CsPbBr_3$-Ptd-L-Ser NCs can be obtained after purification and post ligand-treatment processes using different amounts (20, 40, 80, 120, and 160 µL) of Ptd-L-Ser to optimize the replacement of OA and OLA ligands (**Figure 1**a).

At first, the photophysical properties of the pristine $CsPbBr_3$ and $CsPbBr_3$-Ptd-L-Ser NCs toluene solutions were investigated by steady-state UV–vis absorption and emission spectroscopy as well as time-resolved photoluminescence decay. The absorption band centered at ≈475 nm becomes sharper (better-resolved excitonic features) upon increasing the amount of Ptd-L-Ser (Figure 1b), suggesting the surface derivatization of the initial crystallites becomes uniform and the initial polydispersity in size tends to be smaller.[30] This was also observed in the L-phenylalanine treated $CsPbI_3$[31] and the $CsPbBr_3$ that treated by the size-selection process.[27] Herein, the UV–vis absorption spectrum of the Ptd-L-Ser toluene solution is also measured (Figure S1, Supporting Information), no obvious peak or band can be detected from the spectrum. The emission spectra show ≈ 1–3 nm blueshift upon increasing the amount of Ptd-L-Ser (Figure 1c and **Table 1**). Notably, this blueshift was also reported in the previous literature, in which the pristine MHPs NCs were treated by polyzwitterionic ligands[32,33] and thiocyanate salt.[34] Meanwhile, the NCs show longer decays upon increasing the amount of the Ptd-L-Ser (Figure 1c), suggesting that the incorporated ligands can indeed be helpful for healing the defects on the surface of the $CsPbBr_3$ NCs. Detailed information of the average excited state lifetimes is shown in Table 1.

While $CsPbBr_3$ NCs show a modest PLQY value of ≈65%, this is enhanced with the increasing amount of Ptd-L-Ser, reaching a maximum value of ≈98% for the $CsPbBr_3$-Ptd-L-Ser-120 NCs (Table 1). The radiative recombination rate (k_{rad}) is also gradually enhanced upon increasing the Ptd-L-Ser amount (Table 1). Further increasing the amount of the Ptd-L-Ser (to 160 µL) will cause the slight decreased PLQY, radiative recombination rate, and the lifetime values, while the nonradiative recombination rate and the FWHM show increasing trend (Table 1). Here, the
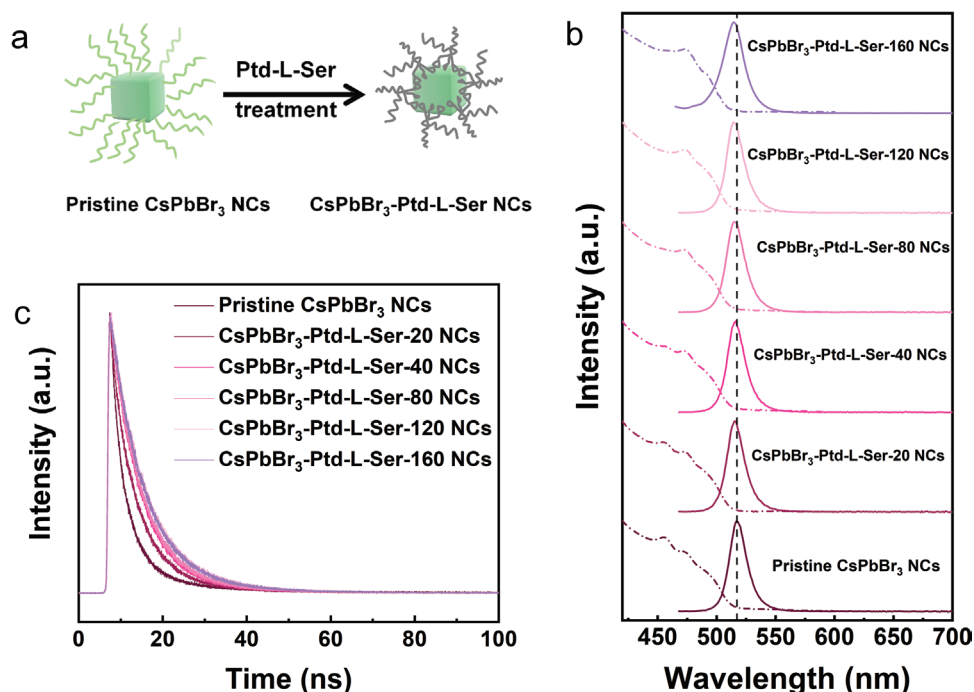
Figure 1. a) Schematic representation of the ligand treatment process. b) Normalized UV–vis absorption and emission spectra and c) photoluminescence decay curves of the pristine CsPbBr$_3$ and CsPbBr$_3$-Ptd-L-Ser NCs (see legend) toluene solutions.

optimized sample CsPbBr$_3$-Ptd-L-Ser-120 NCs will be named as CsPbBr$_3$-Ptd-L-Ser NCs and hereafter used for further analysis and applications.

What is more, the CsPbBr$_3$ NCs show improved stability with the incorporation of Ptd-L-Ser. The CsPbBr$_3$-Ptd-L-Ser NCs toluene solution is very clear and green after one night stirring under ambient condition, while the pristine CsPbBr$_3$ NCs solutions become yellow and turbid under the same conditions (Figure S2, Supporting Information). Then, part of these solutions were transferred to small tubes for the long-time observation (Figure S3, Supporting Information). The CsPbBr$_3$-Ptd-L-Ser NCs solutions can keep clear even after 6 months under ambient conditions. However, the pristine CsPbBr$_3$ NCs solution shows obvious precipitates. Therefore, Ptd-L-Ser can significantly improve both the optical properties through passivating the surface defects and the colloid stability of the CsPbBr$_3$ NCs.

X-ray diffraction (XRD) was then performed to demonstrate the impact of Ptd-L-Ser ligands on the crystal structure of the CsPbBr$_3$ NCs. As shown in **Figure 2**a, the XRD patterns are identical for both films, suggesting no phase transformation induced by the addition of the Ptd-L-Ser ligands (Figure S4 and Table S1, Supporting Information). Fourier-transform infrared (FTIR) spectroscopy was further performed to investigate how Ptd-L-Ser is incorporated onto the surface of CsPbBr$_3$ NCs. As illustrated in Figure 2b, the peaks centered at 2922, 2841, and 1461 cm^{-1} can be noted in all samples. They are assigned to the C–H symmetric and asymmetric stretching and bending modes.[32] Meanwhile, the peaks located at 1058, 1221, 1344, and 1736 cm^{-1} are assigned to the P–O–C, P=O, P=O, P=O–OH stretching and bending modes of the Ptd-L-Ser ligand. They are clearly detected in CsPbBr$_3$-Ptd-L-Ser,[35–37] suggesting that the Ptd-L-Ser ligands have been successfully incorporated onto the surface of the CsPbBr$_3$ NCs. In addition, the O=P–OH and

Table 1. Photoluminescence parameters of the pristine CsPbBr$_3$ NCs and CsPbBr$_3$-Ptd-L-Ser NCs toluene solutions.

Sample	λ_{max}[a,b] [nm]	FWHM[a,b] [nm]	PLQYs[b] [%]	τ[c] [ns]	k_{rad} [×10^{-3} ns^{-1}]	k_{nonrad} [×10^{-3} ns^{-1}]
Pristine CsPbBr$_3$ NCs	517	17	66.34	10.03	66.14	33.56
CsPbBr$_3$-Ptd-L-Ser-20 NCs	515	16	80.04	11.28	70.96	13.69
CsPbBr$_3$-Ptd-L-Ser-40 NCs	515	17	85.20	11.90	71.60	12.44
CsPbBr$_3$-Ptd-L-Ser-80 NCs	515	17	90.89	12.65	71.85	7.20
CsPbBr$_3$-Ptd-L-Ser-120 NCs	514	17	97.73	12.70	76.95	1.79
CsPbBr$_3$-Ptd-L-Ser-160 NCs	514	19	92.23	12.66	72.85	6.13

[a]Maximum wavelength (λ_{max}) and full width at half maximum (FWHM); [b]Excitation wavelength of 450 nm; [c]Excited state lifetimes at excitation wavelength of 450 nm.
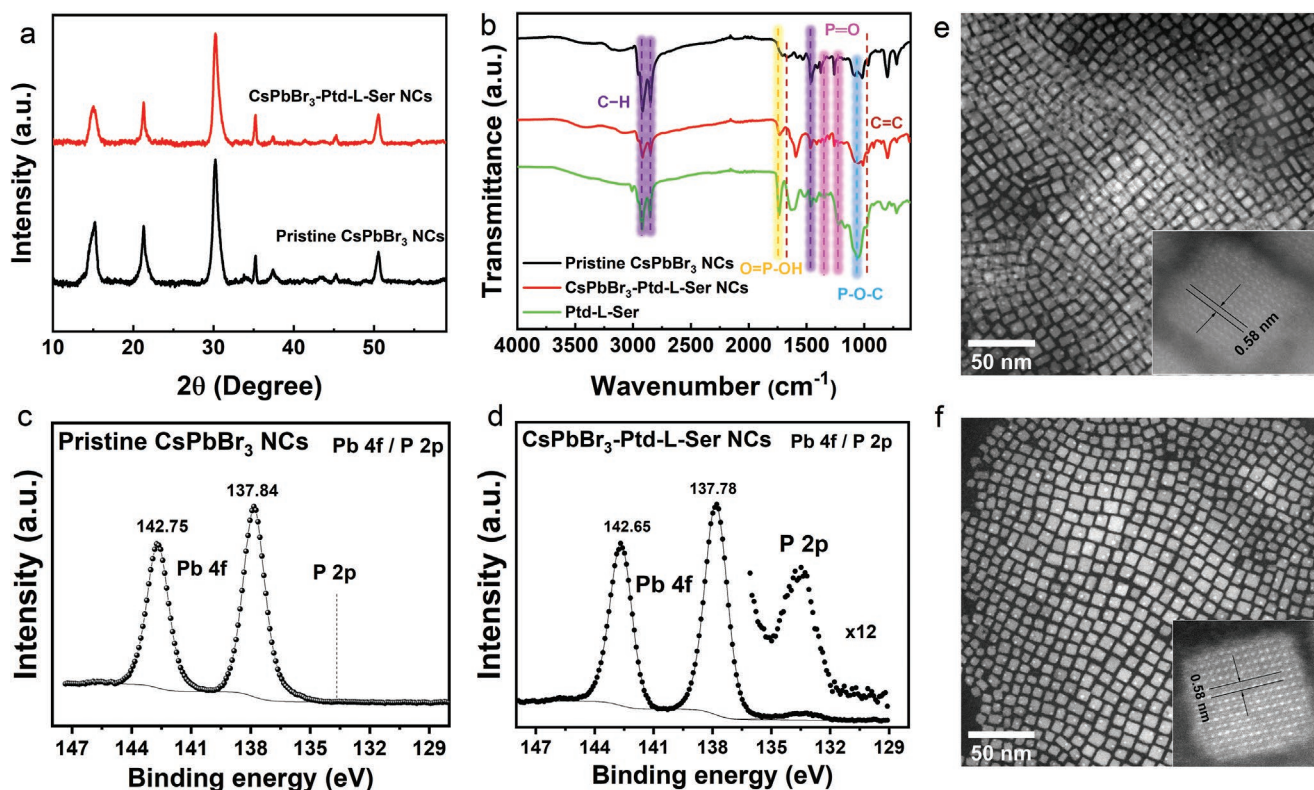
Figure 2. a) The XRD patterns of the pristine $CsPbBr_3$ and the optimized $CsPbBr_3$-Ptd-L-Ser NCs using 120 µL of the ligand for the post functionalization. b) The FTIR spectra collected from the pristine $CsPbBr_3$ NCs, $CsPbBr_3$-Ptd-L-Ser NCs, and the Ptd-L-Ser ligands. High-resolution XPS in the Pd 4f region and P 2p for c) the pristine $CsPbBr_3$ NCs and d) $CsPbBr_3$-Ptd-L-Ser NCs. Here, the signal of the P 2p was enlarged by 12 times because of the low amount. The HAADF-STEM images of e) the pristine $CsPbBr_3$ NCs and f) the optimized $CsPbBr_3$-Ptd-L-Ser NCs. The insets in (e) and (f) present the corresponding high-resolution STEM images of the NCs, with the lattice spacing of 0.58 nm.

P—O—C peaks from $CsPbBr_3$-Ptd-L-Ser NCs move weakly to the lower wavenumber compared with the Ptd-L-Ser ligands, which indicates the chelating effects between $CsPbBr_3$ NCs and the Ptd-L-Ser other than the simple physical adsorption (Figure S5, Supporting Information). Importantly, the peaks at 964 and 1670 cm^{-1} assigned to the C=C bending and stretching modes, are almost absent in the $CsPbBr_3$-Ptd-L-Ser NCs, indicating that most of the OA and OLA ligands have been effectively replaced by Ptd-L-Ser during the post-treatment process.

In addition, X-ray photoelectron spectra (XPS) measurements were also performed to prove the presence of the P in the $CsPbBr_3$-Ptd-L-Ser NCs. As shown in Figure 2d, a clear peak at 133.3 eV in the spectra of $CsPbBr_3$-Ptd-L-Ser NCs is emerged, which can be assigned to the phosphate group in Ptd-L-Ser ligands. However, this spectral signal is absent in the spectrum of pristine $CsPbBr_3$ NCs, since the capping agent used in this case does not contain P (Figure 2c). In addition, a surface chemical analysis was carried out based on the photoelectron peak areas and corresponding sensitivity factors. Table S2 in the Supporting Information shows the relevant atomic ratios. As expected, the C/Pb ratio is high for all samples, confirming the capping of the surface with organic molecules. Specially, the C/Pb atomic ratio increases after the treatment of the Ptd-L-ser ligand, indicating more ligands were incorporated to the surface of the $CsPbBr_3$ NCs. These ligands can be helpful to fill the vacancies or attach to the undercoordinated

ions, which contribute to enhanced optical properties and the excellent colloidal stability. In addition, the Pb 4f peak of the $CsPbBr_3$-Ptd-L-Ser NCs shifts toward lower binding energy compared to the pristine $CsPbBr_3$ NCs while the O 1s peak shift to higher binding energy (Figure 2c,d and Figure S6a, Supporting Information), suggesting that the electron density around Pb increases after the incorporation of the ligands. This further indicates that the strong coordination binding between Pb^{2+} and multiple C=O functional groups.[26,38]

High-angle annular dark field-scanning transmission electron microscopy (HAADF-STEM) was further applied to demonstrate the structural and morphological integrity after the Ptd-L-Ser ligands treatment. As shown in Figure 2e,f, the NCs are all in cubic shape and homogenous distribution. Further size distribution analysis shows the average edge sizes for the pristine $CsPbBr_3$ NCs and $CsPbBr_3$-Ptd-L-Ser NCs are 8.57 ±1.52 and 7.75 ± 1.11 nm, respectively (Figure S7, Supporting Information). The slight lower value can be attributed to the incorporation of the Ptd-L-Ser ligands that prevent the self-rearrangement and the aggregation of the $CsPbBr_3$ NCs as shown in Figure 2e. In addition, a lattice distance of ≈0.58 nm is observed for both cases, corresponding to the (100) plane of the cubic structure. Therefore, the morphology and structure of the NCs are kept after ligand treatment. Finally, transmission electron microscopy (TEM) images with a wide view corroborate the above finding concerning structure and size distribution
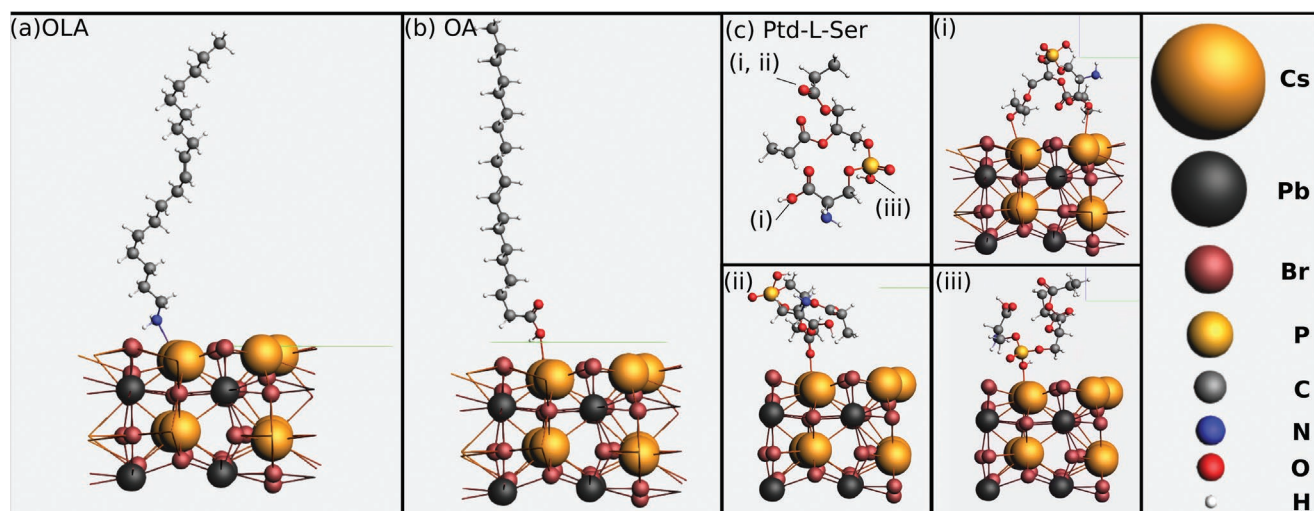
Figure 3. a) OLA, b) OA, and c) Ptd-L-Ser adsorbed on CsPbBr$_3$. Possible sites for the adsorption of Ptd-L-Ser, (i)–(iii) are marked on Ptd-L-Ser in panel (c).

(Figure S8, Supporting Information).To further understand the bonding nature of the Ptd-L-Ser ligand on the surface of CsPbBr$_3$ NCs, DFT calculations were carried out to compare the adsorption energy (E_{ads}) of OLA, OA, and Ptd-L-Ser (**Figure 3**, see the Experimental Section for more details). As the Ptd-L-Ser structure is very big (Figure S9, Supporting Information) and has multiple adsorption sites, we simplified the simulation process through calculating the E_{ads} of the possible sites (Figure 3c). The highest two E_{ads} (absolute value) of Ptd-L-Ser are 583 and 235 meV, while E_{ads} for OLA and OA are 188 and 44 meV, respectively (**Table 2**), confirming the stronger bonding strength for Ptd-L-Ser ligands. A direct comparison of the E_{ads} shows the following order: OA < Ptd-L-Ser iii < OLA < Ptd-L-Ser ii < Ptd-L-Ser i (Table 2). Since Ptd-L-Ser has several binding sites, within Ptd-L-Ser, the most stable adsorption will be via site i and ii (Figure 3c). In addition, the bond length along adsorption site (B$_A$) and nearest neighboring atoms (B$_n$) for molecular systems adsorbed on CsPbBr$_3$ are also calculated (**Table 3**). The same feature is also reflected in shorter bond lengths between Ptd-L-Ser and perovskite surface at the adsorption sites (ranging from 2.59 to 2.75 Å), in comparison to bonds lengths of 3.01 and 3.20 Å, as formed by the adsorption of OLA and OA (Table 3). Hence, we conclude that the incorporation of Ptd-L-Ser ligands can indeed stabilize CsPbBr$_3$ NCs due to: i) multiple possible allowed bonding sites, which enhance chances of adsorption and ii) stronger bonds at the adsorption sites. In addition, the simulated XRD shows good match with the experimental XRD pattern for CsPbBr$_3$ (see Figures S10

and S11, Supporting Information, for more details). The direct bandgap (the energy difference between the highest valence band edge and lowest conduction band edge) of CsPbBr$_3$ using meta-generalized gradient approximation (GGA) M06L exchange correlation functional, was calculated to be 2.19 eV. Adsorption of OA, OLA, and Ptd-L-Ser ligands on CsPbBr$_3$ (100) slab results in the saturation of some dangling bonds and lead to slight increase in the bandgap, amounting to indirect bandgap of 2.695 ± 0.095 eV. No significant change is noted in the electronic structure after the post ligand-adsorption. This suggests that the adsorption of the ligands does not modify the bandgap of the material significantly.

2.2. Fabrication and Characterization of CsPbBr$_3$-Ptd-L-Ser-Based Color Filters

The excellent photophysical properties and the colloidal stability encourage us to further fabricate color filters for pc-LEDs. They were prepared through directly dispersing the same amount of CsPbBr$_3$ (**1**) and CsPbBr$_3$-Ptd-L-Ser (**2**) NCs in a polystyrene

Table 2. E_{ads} and bandgap for molecular systems adsorbed on CsPbBr$_3$.

System	Bandgap with interaction [eV]	E_{ads} [eV]
OLA	2.73	0.188
OA	2.60	0.044
Ptd-L-Ser i	2.77	0.583
Ptd-L-Ser ii	2.79	0.235
Ptd-L-Ser iii	2.67	0.179

Table 3. B$_A$ and B$_n$ for molecular systems adsorbed on CsPbBr$_3$.

System	B$_A$ [Å]	B$_n$ [Å]
OLA	N$_{95}$-Cs$_{11}$: 3.01	Cs$_{11}$-Br$_{27}$: 3.65
		Cs$_{11}$-Br$_{28}$: 3.97
OA	O$_{50}$-Cs$_{68}$: 3.20	Cs$_{68}$-Br$_{84}$: 3.54
		Cs$_{68}$-Br$_{85}$: 4.01
Ptd-L-Ser i	O$_{10}$-Cs$_{57}$: 2.59	Cs$_{57}$-Br$_{73}$: 3.65
	O$_{17}$-Cs$_{60}$: 3.44	Cs$_{57}$-Br$_{74}$: 3.97
		Cs$_{60}$-Br$_{76}$: 3.53
		Cs$_{60}$-Br$_{74}$:4.05
Ptd-L-Ser ii	O$_{10}$-Cs$_{57}$: 2.73	Cs$_{57}$-Br$_{73}$: 3.6
		Cs$_{57}$-Br$_{74}$: 3.93
Ptd-L-Ser iii	O$_{22}$-Cs$_{57}$: 2.75	Cs$_{57}$-Br$_{73}$: 3.63
		Cs$_{57}$-Br$_{74}$: 3.97
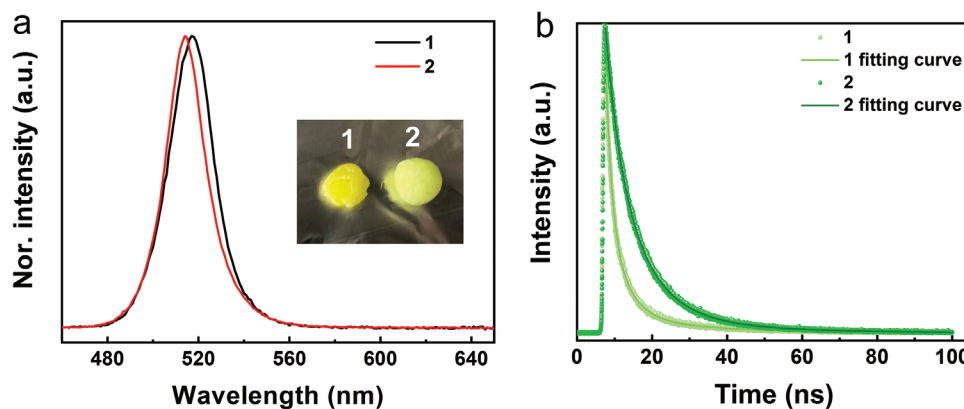
Figure 4. a) Normalized emission spectra and b) emission decay curves of **1** and **2** filters. Inset in (a) is a photograph of the **1** (left) and **2** (right) filters.

saturated toluene solution that was dried under vacuum. As shown in the inset of **Figure 4**a, both filters were yellowish to the naked eye. **2** shows a slightly blue-shifted emission compared to that of **1**, but the PLQY is retained (≈90%) upon film forming. In contrast, the PLQY of **1** is strongly reduced to 30% (i.e., 50% loss) along with a wide FWHM of 23 nm due to the desorption of OA and OLA capping ligands, increasing surface traps as well as the undercoordinated ions. This was further confirmed by the shorter τ values of **1**, suggesting that the Ptd-L-Ser ligand capping is efficient in preventing CsPbBr$_3$ NCs' degradation/aggregation upon film forming (Figure 4b and **Table 4**). Final confirmation comes from the direct comparison of the loss of radiative recombination rate and the increase of nonradiative recombination rate between the filters and their respective solutions. Here, **2** holds up to ≈90%, while **1** loses more than 50% of, for example, the radiative recombination rate (Tables 1 and 4).

Next, the stabilities of **1** and **2** filters against surrounding stresses, including heat, water, and oxygen over time were evaluated. The thermal stability was first investigated through monitoring the emission intensity upon increasing the temperature up to 100 °C (**Figure 5**). The emission of the **1** filter exponentially reduces, reaching losses of 80% at 60 °C (Figure 5a,c). This goes hand-in-hand with a severe redshift of the maximum emission (Figure S13a, Supporting Information). In sharp contrast, **2** filter shows significantly improved thermal stability with a linear-like decay that retains ≈60% of the initial emission at 60 °C (Figure 5b,c). This thermal behavior can be rationalized by the activation energy for exciton dissociation (exciton binding energy, E_b). In short, the temperature dependent emission intensity can be fitted by the following Arrhenius equation[1,26,39]

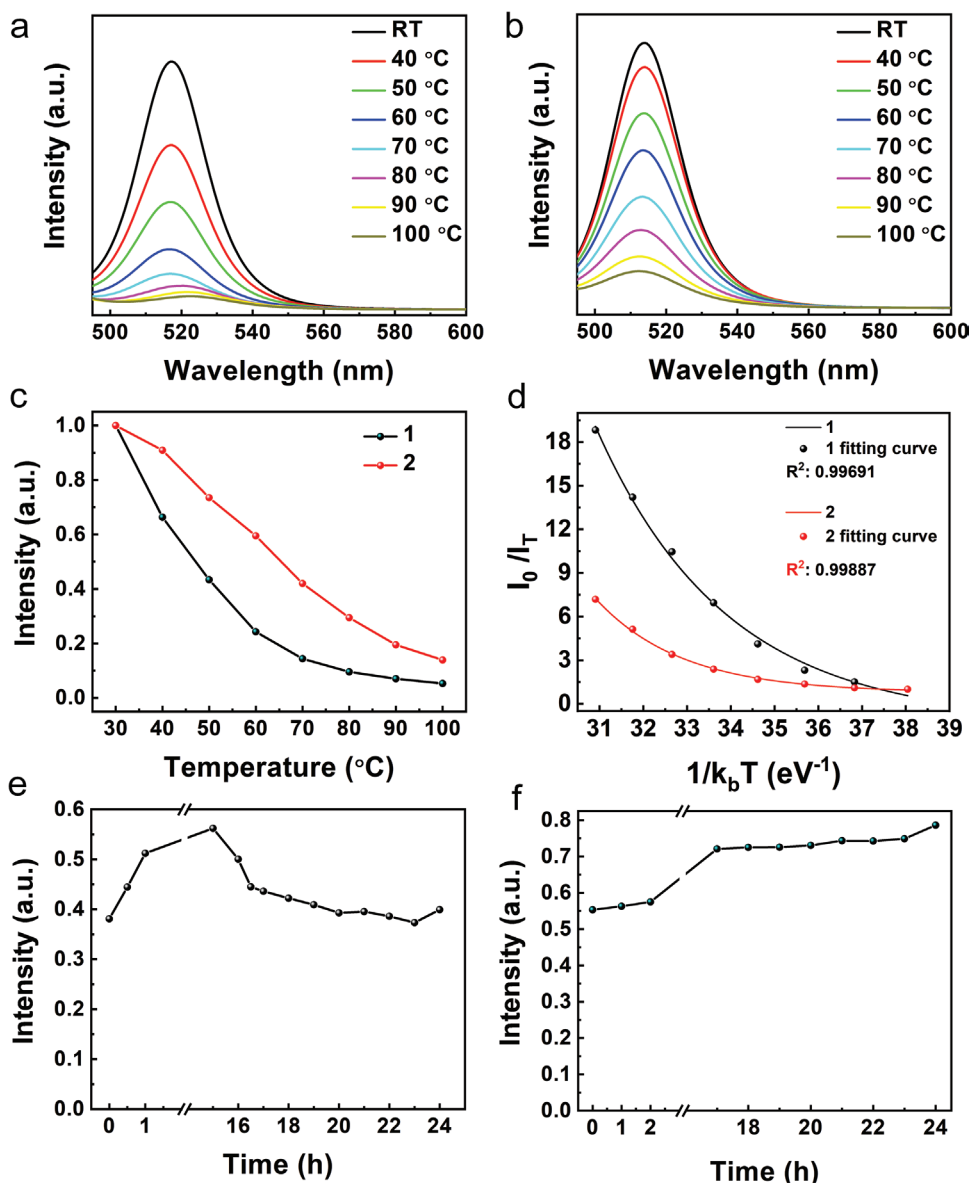$$I_T = \frac{I_0}{1 + Ae^{\frac{-E_b}{k_b T}}} \quad (1)$$

Table 4. Photoluminescence parameters of pristine CsPbBr$_3$ (**1**) and CsPbBr$_3$-Ptd-L-Ser (**2**) NCs based filters.

Filter	PLQYs[a] [%]	FWHM [nm]	τ[a] [ns]	k_{rad} [×10^{-3} ns^{-1}]	k_{nonrad} [×10^{-3} ns^{-1}]
1	32.39	23	10.55	30.70	64.08
2	88.05	18	12.96	67.94	9.22

[a]Excitation wavelength of 450 nm.

where I_0 and I_T are the initial photoluminescence (PL) intensity and the PL intensity at the testing temperature, respectively. k_b and A are the Boltzmann constant and the pre-exponential coefficient, respectively. The fitting is presented in Figure 5d, through collecting the ratio of I_0/I_T and the reciprocal of the photon energy (eV^{-1}). The calculated E_b are 337.4 ± 27 and 507.39 ± 20 meV for **1** and **2** filters, respectively. Higher E_b usually contributes to a more prominent radiative recombination rate,[40] which is favorable for LED applications. Finally, the emission recovery processes were also monitored under dark conditions. As shown in Figure 5f, ≈80% of the initial emission intensity can be recovered for **2** filters after 24 h, while the emission band shape is also recovered (Figure S13d, Supporting Information). Notably, the loss of the emission intensity and the emission band of **1** filter is irreversible (Figure 5e and Figure S13c, Supporting Information), suggesting a severe degradation and/or aggregation. This is consistent with the previous works, in which the dynamic equilibrium of adsorption and desorption of ligands can be easily accelerated at higher temperatures,[17] leading to the aggregation of the MHPs NCs and the decreased emission intensity. The thermal stability of the filters was also assessed at continuous 60 °C over time (Figure S14, Supporting Information). Again, **1** filter undergoes considerable emission intensity drop (>60% after 24 h). However, **2** filters show a significant improvement in the stability without any loss after 48 h. Therefore, the above results reveal that Ptd-L-Ser not only enhances the thermal resistance for increasing temperature but also results in increased resistance under long-term thermal treatment.

The storage stability of these filters under ambient conditions was further examined (**Figure 6**a). The PLQY of **1** filter reduces to ≈10% after 1 month, along with a severe redshift in the emission peak (Figure 6d). In contrast, **2** filters hold a high PLQY value of ≈80% after half year. Meanwhile, the emission peak does not show obvious change over time (Figure 6c). Therefore, the Ptd-L-Ser ligand can significantly shield the CsPbBr$_3$ NCs, leading to outstanding air stability. Here, water stability is one of the widely used assessment criteria for the MHPs, since water or even moisture will cause aggregation and decomposition of MHPs. The emission of **1** filters is almost quenched after half year storage in water, whereas **2** filters hold their emission features with PLQY values at ≈53% (Figure 6b). This points out that the dynamic adsorption/desorption of

**ADVANCED
SCIENCE NEWS**

www.advancedsciencenews.com

**ADVANCED
OPTICAL
MATERIALS**

www.advopticalmat.de

Figure 5. Temperature-dependent emission spectra of a) **1** and b) **2** filters showing c) a direct comparison of the intensity evolution upon increasing temperature and d) the analysis of the emission intensity trend versus the reciprocal of the photon energy for **1** and **2** filters. The changes in the emission intensities during of the recovery process for e) **1** and f) **2** filters are also presented.
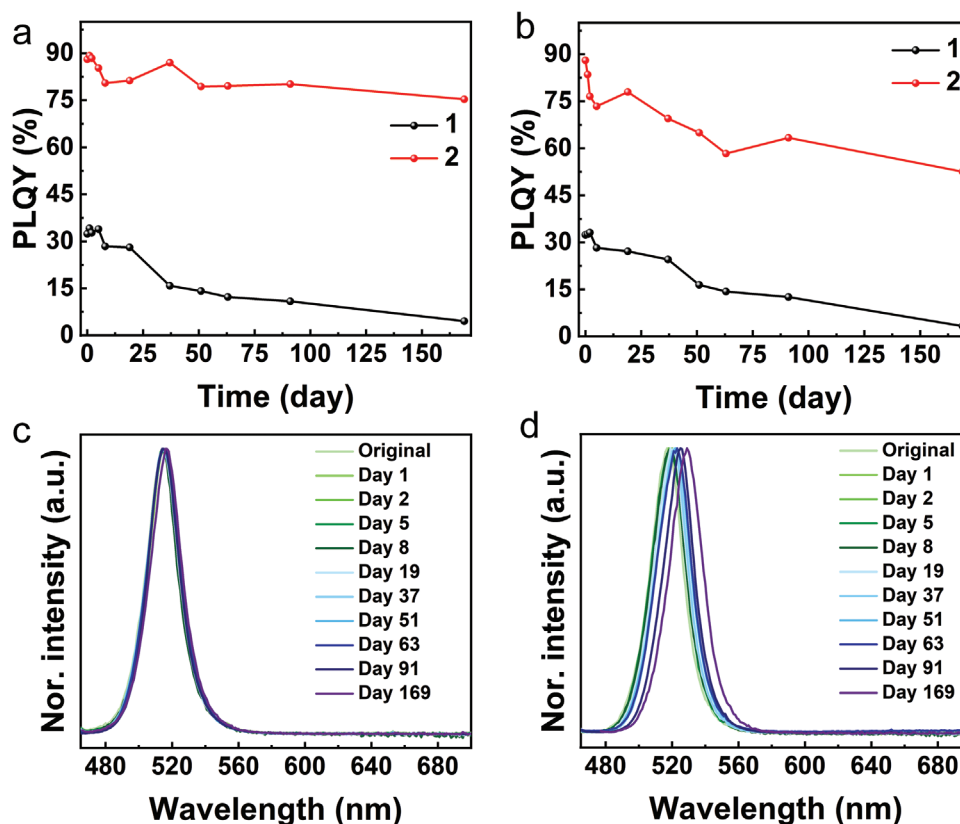
Ptd-L-Ser ligands onto the surface of $CsPbBr_3$ NCs is slowed down compared to conventional capping agents, decreasing the permeation of the water into the surface of the $CsPbBr_3$ NCs.

2.3. Fabrication and Characterization of the pc-LEDs

Green pc-LEDs were fabricated via putting **1** and **2** filters on a blue emissive LED chip (440 nm) in a remote configuration (**Figure 7**a)—see the Experimental Section. In line with the photophysical features, Figure 7b shows an enhanced luminous efficiency for **2**-pc-LEDs compared to **1** device regardless of the applied current range (10–150 mA). In particular, a maximum value of ≈65 lm W^{-1} is achieved at 20 mA and is slowly

decaying to ≈50 lm W^{-1} at 150 mA for **2** devices, while **1** devices reach 45 lm W^{-1} at 20 mA with a more pronounced linear decay to 27 lm W^{-1} at 150 mA. The evolution of the emission spectra during the tests was also monitored (Figure S15, Supporting Information). In both devices, the emission intensity increases upon increasing current without the changes in either location or shape of emission peaks, suggesting that both filters are stable under short-term illumination.

Next, the stabilities of the green pc-LEDs were evaluated under ambient conditions, through monitoring the time to reach half of the initial emission ($T_{1/2}$) under low (20 mA) and high (100 mA) applied currents. Meanwhile, the changes in the emission spectra (both the shape and maximum) were also recorded over time. **1** devices show $T_{1/2}$ of ≈120 h under 20 mA

**ADVANCED
SCIENCE NEWS**

www.advancedsciencenews.com

**ADVANCED
OPTICAL
MATERIALS**

www.advopticalmat.de

Figure 6. a) Air and b) water stabilities of **1** and **2** filters, through monitoring the PLQYs for half year. Normalized emission spectra of c) **2** and d) **1** filters during storing in air.

(Figure 7c), in which the emission band shows a gradual redshift that is attributed to the aggregation of the $CsPbBr_3$ NCs caused by the desorption of the OA and OLA ligands (Figure S16a,b, Supporting Information). **2** pc-LEDs show no decrease of the emission intensity and/or change of the emission band shape for >700 h (Figure 7c and Figure S16c,d, Supporting Information), which is superior to the prior-art using nonbiogenic ligands as capping agents for $CsPbBr_3$ testing under the same current (e.g., 50% of the initial brightness loses after 546 h at 20 mA).[28] Notably, the initially increased emission is attributed to the trap healing effect caused by the illumination through removing the dangling ligands.[8] Thispassivation effect was proved by the XPS measurements. There is a clear peak at 133.3 eV in the spectra of $CsPbBr_3$-Ptd-L-Ser before and after the light treatment that can be assigned to the phosphate group in Ptd-L-Ser (Figure S6b, Supporting Information). The Ptd-L-Ser capping seems to be stable to the light treatment since the P/Pb ratio (Table S2, Supporting Information) does not change for the light-treated sample. However, the C/Pb ratio shows a slight decrease, which may be caused by the removal of the dangling ligands or the uncertainties caused by the adventitious C.

This passivation effect is also validated by the emission decay measurements after the light treatment. As shown in Figure S18 in the Supporting Information, the blue light treated **2** filter shows a slower decay compared with the as-prepared one, indicating longer lifetime (13.45 ns). Meanwhile, the blue light treated **2** filter also demonstrates a higher PLQY of 92.5%.

The calculated radiative recombination rate (k_{rad}) and the nonradiative recombination rate (k_{nonrad}) are 68.77×10^{-3} and 5.58×10^{-3} ns^{-1}, respectively. The blue light treated **2** filter shows reduced nonradiative recombination rate compared with the as-prepared **2** filter. All these results prove that the passivation effect caused by the initial irradiation. On the other hand, some shallow level trap states like vacancies are always existing on the MHP's surface because of the fact that the surface of the perovskites is not totally defect-free. O^{2-} species are generated through the reaction between the photoexcited electrons from the $CsPbBr_3$ NCs and molecular oxygen under ambient condition during the operational stability measurements. The negatively charged O^{2-} species can bind with the defects, such as Br vacancies (positively charged), leading to the subsequent enhancement in the photoluminescence.[41,42] The combination of the photoinduced trap sites and the self-healing effect by the Ptd-L-Ser ligands, as well as the combination of the O^{2-} species and the surface traps may be responsible for the fluctuation in the emission intensity during the long-term measurements, and therefore the outstanding operational stability under 20 mA. At high applied currents of 100 mA, **2** pc-LEDs still show a very promising operational stability of 210 h compared to that of 27 h for **1** devices (Figure 7d), highlighting the successful stabilization effect of the biogenic Ptd-L-Ser ligands on the $CsPbBr_3$ NCs even under device operational conditions.

The excellent operational stability and the available high quality of the green filters promote their potential to be used in the
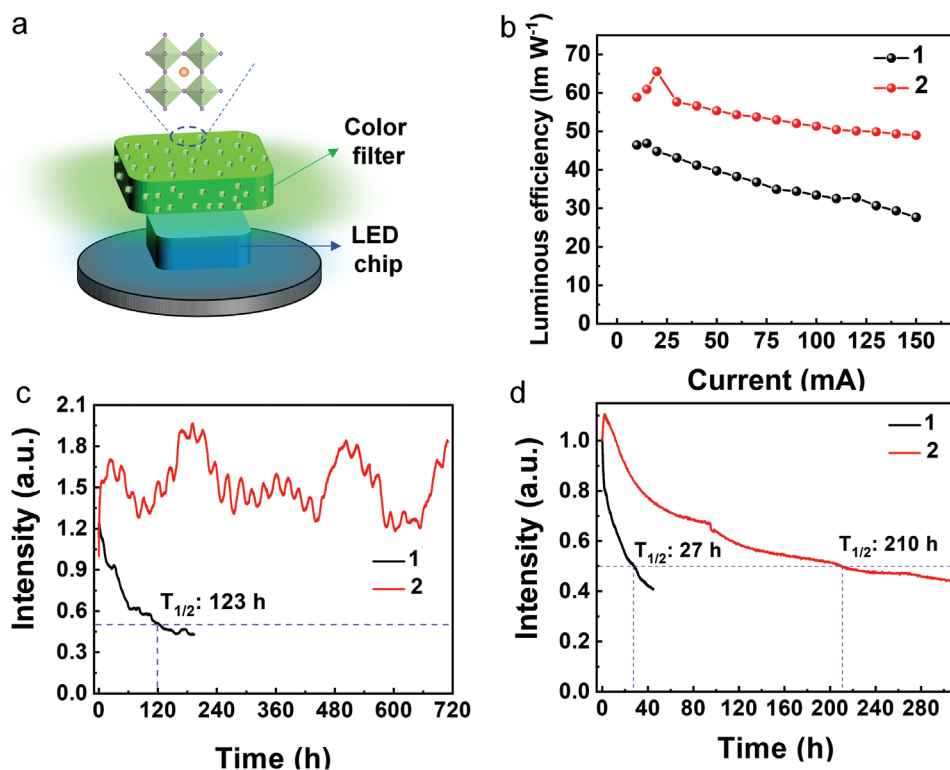
Figure 7. a) The schematic of the green pc-LEDs, combining the blue LED chip (440 nm) with the green filter in a remote configuration. b) Direct comparison of the luminous efficiency upon increasing the applied current. Emission intensity decays at c) 20 and d) 100 mA of green pc-LEDs fabricated with **1** and **2** filters.

display technology. WLEDs devices were successfully fabricated by using the blue LED chip, green emissive $CsPbBr_3$-Ptd-L-Ser combined with the commercial red emissive K_2SiF_6:Mn^{4+} (KSF). **Figure 8**a illustrates the electroluminescence spectra of the device. The optical image of the working WLED device emitting bright white light under 20 mA is demonstrated in the inset, with x/y Comission Internationale de l'Éclairage (CIE) color coordinates of 0.34/0.33 (Figure 8b). The pc-WLEDs cover 125.2% bigger area than that of the National Television Systems Committee (NTSC) standard. The highest luminous efficiency of 76 lm W^{-1} is about two times higher than that one using the nonbiogenic capped $CsPbBr_3$ NCs (Figure 8c).[28] The evolution of the spectra under increasing current is shown in Figure S19a in the Supporting Information. Finally, the WLED devices show an outstanding stability with $\Delta x/y$ of ± 0.01 over several weeks under operational conditions (Figure 8d and Figure S19b, Supporting Information).
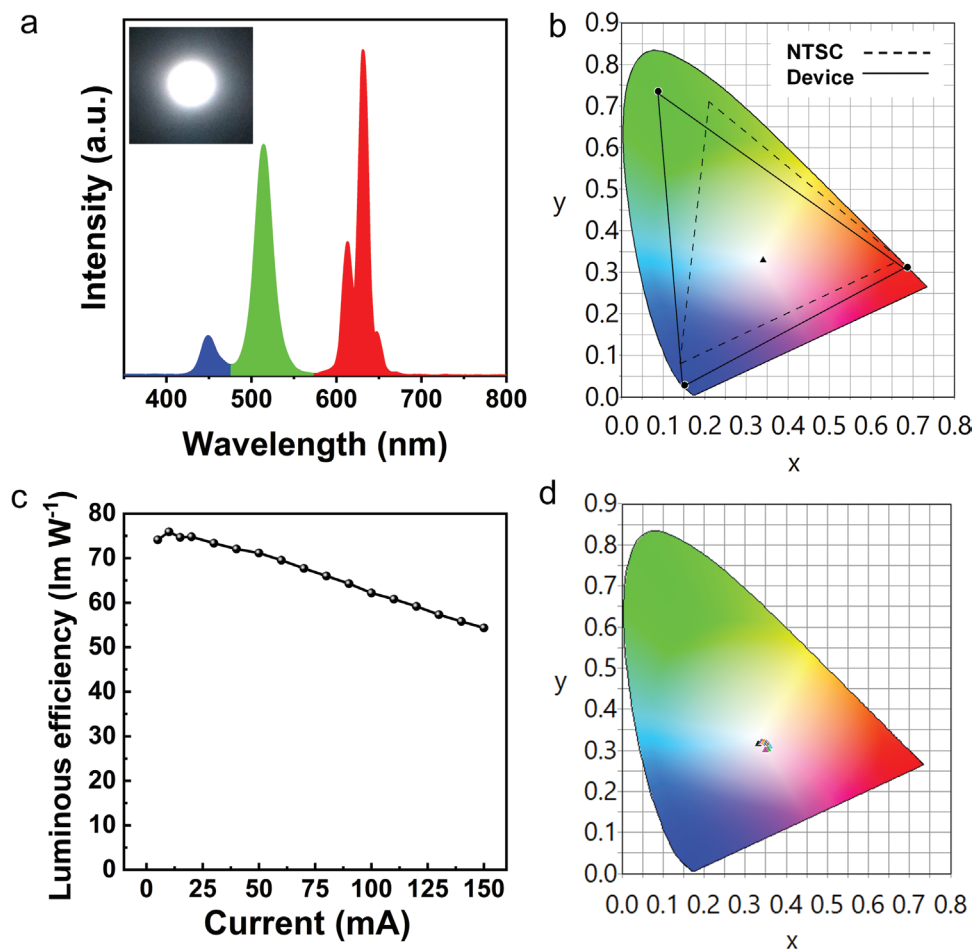
3. Conclusions

This work demonstrates the first use of biogenic capping ligands (Ptd-L-Ser) that can effectively improve the PLQY (>90% vs <30%) and colloidal stability (half year vs <1 week) of the $CsPbBr_3$ NCs due to the increased exciton binding energy without causing any phase transformation. This was confirmed by DFT calculations, in which Ptd-L-Ser ligands featured stronger binding energies through forming multiple adsorption sites compared to those of reference ligands

(OA and OLA). This is also reflected in polymer filters with excellent thermal stabilities (stable emission at 60 °C for 2 d), storage (high PLQY of more than 75% over about half year), and water (keeping PLQY value of >52% after 169 d). The incorporation of the Ptd-L-Ser ligands was also effective to realize pc-LEDs with a high luminous efficiency of >65 lm W^{-1} and outstanding stability of >700 h (20 mA) and 210 h (100 mA) under ambient device operational conditions, representing almost one order of magnitude enhancement compared to reference devices with pristine $CsPbBr_3$ NCs (45 lm W^{-1}; 120 h@20 mA) as well as the prior-art ligand@$CsPbBr_3$ device (average 50 lm W^{-1} and <200 h@20 mA). Furthermore, the WLEDs fabricated with the $CsPbBr_3$-Ptd-L-Ser NCs exhibit a wide gamut, high luminous efficiency of 76 lm W^{-1}, and outstanding color stability over weeks under operational conditions. All-in-all, this work sets in that the rational ligand engineering of biogenic capping ligands is an efficient strategy to improve the photophysical properties as well as the stability of the MHPs.

4. Experimental Section

Chemicals: Cs_2CO_3 (99%), $PbBr_2$ (trace metals basis, 99.999%), OA (technical grade, 90%), ODE (technical grade, 90%), OLA (technical grade, 70%), toluene (anhydrous, 99.8%), ethyl acetate (EA, anhydrous, 99.8%), PS (average $M_w \approx 350\,000$, average $M_n \approx 170\,000$) were obtained from Sigma-Aldrich. Phosphatidyl-L-serine (Ptd-L-Ser) was purchased from Biosynth Carbosynth. All chemicals were used as received without further treatment.

**ADVANCED
SCIENCE NEWS**

www.advancedsciencenews.com

**ADVANCED
OPTICAL
MATERIALS**

www.advopticalmat.de

Figure 8. a) The emission spectra of the WLEDs devices combining the blue LED chip, the green CsPbBr$_3$-Ptd-L-Ser NCs and the red KSF. Inset is the photograph of the working device under 20 mA. b) The CIE color coordinates corresponding to the WLED devices (solid line) and the NTSC standard (dotted line). c) The luminous efficiency of the WLED devices under increasing applied currents. d) The evolution of the color coordinates of the WLEDs device under working conditions over weeks.

Synthesis and Purification of Pristine CsPbBr$_3$ NCs: The pristine CsPbBr$_3$ NCs were prepared following the literature with minor modifications.[6] EA was introduced to the crude solution with a volume ratio of 3:1 (EA to crude solution) to precipitate the NCs. Then, the solution was centrifuged at 8000 rpm for 8 min. The supernatant was discarded and the precipitates were redispersed in toluene. Another round of centrifugation at 5000 rpm for 4 min was applied to remove big particles and unreacted precursors. Then, the supernatant with a total volume of 10 mL was obtained and stored for further use.

Preparation of the CsPbBr$_3$-Ptd-L-Ser NCs: First, Ptd-L-Ser toluene solution (0.05 м) was obtained through dissolving Ptd-L-Ser (39.6 mg, 0.05 mmol) in toluene (1 mL). The above purified NCs toluene solution was divided equally to five vials (2 mL in each vial). Then, different volumes (20, 40, 80, 120, and 160 μL) of the Ptd-L-Ser toluene solution was added to the vials. The mixture and the pristine toluene solution were stirred overnight under ambient conditions. Here, the Ptd-L-Ser can be effectively grafted to the CsPbBr$_3$ NCs' surface. Finally, another round of centrifugation at 8000 rpm, 5 min was applied to remove the extra ligands.

Fabrication and Characterization of pc-LEDs: 60 μL of the CsPbBr$_3$-Ptd-L-Ser NCs and the pristine CsPbBr$_3$ NCs toluene solutions were thoroughly dispersed in 0.6 mL of PS toluene solution (1 g mL^{-1}). Then, the filters can be obtained when toluene was totally removed under vacuum at room temperature. The pc-LEDs were fabricated through putting the filters above the blue LED chip (440 nm, 3 W) in a remote configuration (1.5 cm between the LED chip and the filter).

The WLEDs were fabricated combining the blue LED chip with the commercial red KSF and the green CsPbBr$_3$-Ptd-L-Ser NCs. The above mixture of the CsPbBr$_3$-Ptd-L-Ser NCs and the PS toluene solution was dropped on the quartz with a size of 1.5 cm × 1.5 cm and then dried under vacuum. The filter was first treated by the blue light for 7 h to get the maximal emission intensity. The KSF powders (120 mg) were mixed with the UV cure adhesion (200 μL, Ossila, E132) and then casted on the quartz (1.5 cm × 1.5 cm), followed by a UV curing process using the UV lamp (302 nm, 3 W). Then, the WLEDs devices can be fabricated through putting the KSF and the CsPbBr$_3$-Ptd-L-Ser NCs filters on the blue LED chip in sequence, keeping the distance between the LED chip and the red filter at 0.5 cm.

A Keithley 2231A-30-3 triple channel DC was used to provide the current source for the LEDs, while the changes in the emission spectra were monitored over time using an AvaSpec-2048L (Avantes) in conjunction with a calibrated integrated Avasphere 30-Irrad. The temperatures of the filters were precisely monitored using a thermographic camera ETS 320 (FLIR systems, Inc) during the thermal stability tests.

Characterization Techniques: The morphology of the NCs was investigated by TEM (FEI Talos F200X microscope, 4K*4K Ceta Camera) and HAADF-STEM (using the STEM mode). The NCs toluene solutions were directly dropped on the grids and dried under ambient condition for the tests. The crystal structure of the NCs was identified by XRD (Philip X' Pert PRO), using a Ni filter and Cu K_α radiation source

($\lambda = 0.154$ nm). The samples were prepared through dropping the NCs toluene solutions on quartz substrates and drying the films at 80 °C in the glove box. The FTIR spectroscopy (Nicolet iS50) measurements were operated using the Attenuated total reflectance mode. XPS were recorded with a lab-based spectrometer (from SPECS GmbH, Berlin) using monochromated Al K_α source (h_v = 1486.6 eV) operated at 50 W as the excitation source. The detailed measurement process can be found in the Supporting Information. UV–vis absorption spectra of the NCs toluene solutions were detected through the UV-2600 spectrometer (Shimadzu). 200 µL of the toluene solution was mixed with 2 mL of toluene to get a desired concentration before testing. The emission spectra, the time-resolved photoluminescence decay, and the PLQYs of both the NCs toluene solutions and the filters were tested by an FS5 Spectrofluorometer (Edinburgh Instruments).

The decay curves can be fitted following the following function[43]

$$I = \sum_n A_n \exp\left(-t / \tau_n\right) \qquad n = 1, 2, 3 \cdots \qquad (2)$$

The average lifetime can be determined by the following formula

$$\tau_{avg} = \frac{\sum_n A_n \tau_n^2}{\sum_n A_n \tau_n} \qquad n = 1, 2, 3 \cdots \qquad (3)$$

Herein, I is the normalized PL intensity and A_n is the amplitude of the decay related lifetime τ_n.

The radiative recombination rate (k_{rad}) and the nonradiative recombination rate (k_{nonrad}) for these NCs toluene solutions and filters were calculated using the equations[29,44]

$$\tau_{avg} = \frac{1}{k_{nonrad} + k_{rad}} \qquad (4)$$

$$PLQY = \frac{k_{rad}}{k_{rad} + k_{nonrad}} \qquad (5)$$

The detailed processes for the measurements of PLQYs for both the solutions and filters can be found in the Supporting Information.

DFT Calculations: The electronic structure and adsorption energy (E_{ads}) calculations reported here were carried out using DFT methodology implemented in Amsterdam Density Functional (ADF)-BAND program.[45] The calculation of optimized geometry and electronic structure for CsPbBr$_3$ was performed using GGA with modified Perdew–Burke–Ernzerhof (mPBE) exchange correlation functional GGA-mPBE as it incorporates both short- and long-range interactions, as well as triplezeta basis sets. CsPbBr$_3$ is known to take up the cubic *Pm-3m* crystal structure with $a = 6.01$ Å.[46] To calculate and compare the adsorption energies on adsorption of OLA, OA, and Ptd-L-Ser; a $2 \times 2 \times 2$ super cell was generated and slab (100) was used to adsorb the molecules as shown in Figure 3. Note that, the long alkyl chain group in Ptd-L-Ser was reduced to ethyl group to optimize the computational cost. E_{ads} was given as follows

$$E_{ads} = E_{ligand+surface} - E_{ligand} - E_{surface} \qquad (6)$$

where $E_{ligand+surface}$, E_{ligand}, and $E_{surface}$ are the formation energies of ligand on surface, isolated ligand, and bare surface, respectively.

Supporting Information

Supporting Information is available from the Wiley Online Library or from the author.

Acknowledgements

Conflict of Interest

The authors declare no conflict of interest.

Data Availability Statement

The data that support the findings of this study are available from the corresponding author upon reasonable request.

Keywords

[1] M. Liu, Q. Wan, H. Wang, F. Carulli, X. Sun, W. Zheng, L. Kong, Q. Zhang, C. Zhang, Q. Zhang, S. Brovelli, L. Li, *Nat. Photonics* **2021**, *15*, 379.

[2] Y. Hassan, J. H. Park, M. L. Crawford, A. Sadhanala, J. Lee, J. C. Sadighian, E. Mosconi, R. Shivanna, E. Radicchi, M. Jeong, C. Yang, H. Choi, S. H. Park, M. H. Song, F. De Angelis, C. Y. Wong, R. H. Friend, B. R. Lee, H. J. Snaith, *Nature* **2021**, *591*, 72.

[3] S.-J. Woo, J. S. Kim, T.-W. Lee, *Nat. Photonics* **2021**, *15*, 630.

[4] M. Vasilopoulou, A. Fakharuddin, F. P. García de Arquer, D. G. Georgiadou, H. Kim, A. R. b. Mohd Yusoff, F. Gao, M. K. Nazeeruddin, H. J. Bolink, E. H. Sargent, *Nat. Photonics* **2021**, *15*, 656.

[5] H. Tsai, S. Shrestha, R. A. Vilá, W. Huang, C. Liu, C.-H. Hou, H.-H. Huang, X. Wen, M. Li, G. Wiederrecht, Y. Cui, M. Cotlet, X. Zhang, X. Ma, W. Nie, *Nat. Photonics* **2021**, *15*, 843.

[6] L. Protesescu, S. Yakunin, M. I. Bodnarchuk, F. Krieg, R. Caputo, C. H. Hendon, R. X. Yang, A. Walsh, M. V. Kovalenko, *Nano Lett.* **2015**, *15*, 3692.

[7] X. Wang, Y. Wang, Y. Chen, X. Liu, Y. Zhao, *Adv. Mater.* **2021**, *33*, 2103688.

[8] Y. Duan, C. Ezquerro, E. Serrano, E. Lalinde, J. García-Martínez, J. R. Berenguer, R. D. Costa, *Adv. Funct. Mater.* **2020**, *30*, 2005401.

[9] Q. A. Akkerman, G. Raino, M. V. Kovalenko, L. Manna, *Nat. Mater.* **2018**, *17*, 394.

[10] Y. Duan, D. Y. Wang, R. D. Costa, *Adv. Funct. Mater.* **2021**, *31*, 2104634.

[11] Y. Wei, Z. Cheng, J. Lin, *Chem. Soc. Rev.* **2019**, *48*, 310.

[12] X. Li, Y. Wu, S. Zhang, B. Cai, Y. Gu, J. Song, H. Zeng, *Adv. Funct. Mater.* **2016**, *26*, 2435.

[13] H. Cho, Y. H. Kim, C. Wolf, H. D. Lee, T. W. Lee, *Adv. Mater.* **2018**, *30*, 1704587.

[14] W. Lv, L. Li, M. Xu, J. Hong, X. Tang, L. Xu, Y. Wu, R. Zhu, R. Chen, W. Huang, *Adv. Mater.* **2019**, *31*, 1900682.

[15] Y. Duan, G. Z. Yin, D. Y. Wang, R. D. Costa, *ACS Appl. Mater. Interfaces* **2021**, *13*, 21800.

[16] C. Sun, Y. Zhang, C. Ruan, C. Yin, X. Wang, Y. Wang, W. W. Yu, *Adv. Mater.* **2016**, *28*, 10088.

[17] J. De Roo, M. Ibanez, P. Geiregat, G. Nedelcu, W. Walravens, J. Maes, J. C. Martins, I. Van Driessche, M. V. Kovalenko, Z. Hens, *ACS Nano* **2016**, *10*, 2071.

[18] J. Shamsi, A. S. Urban, M. Imran, L. De Trizio, L. Manna, *Chem. Rev.* **2019**, *119*, 3296.

[19] F. Krieg, S. T. Ochsenbein, S. Yakunin, S. Ten Brinck, P. Aellen, A. Suess, B. Clerc, D. Guggisberg, O. Nazarenko, Y. Shynkarenko, S. Kumar, C. J. Shih, I. Infante, M. V. Kovalenko, *ACS Energy Lett.* **2018**, *3*, 641.

[20] C. Zhang, J. Chen, L. Kong, L. Wang, S. Wang, W. Chen, R. Mao, L. Turyanska, G. Jia, X. Yang, *Adv. Funct. Mater.* **2021**, *31*, 2100438.

[21] J. Hou, P. Chen, A. Shukla, A. Krajnc, T. Wang, X. Li, R. Doasa, L. H. G. Tizei, B. Chan, D. N. Johnstone, R. Lin, T. U. Schülli, I. Martens, D. Appadoo, M. S. Ari, Z. Wang, T. Wei, S.-C. Lo, M. Lu, S. Li, E. B. Namdas, G. Mali, A. K. Cheetham, S. M. Collins, V. Chen, L. Wang, T. D. Bennett, *Science* **2021**, *374*, 621.

[22] L. Y. Wu, Y. F. Mu, X. X. Guo, W. Zhang, Z. M. Zhang, M. Zhang, T. B. Lu, *Angew. Chem., Int. Ed.* **2019**, *58*, 9491.

[23] J. Hou, Z. Wang, P. Chen, V. Chen, A. K. Cheetham, L. Wang, *Angew. Chem., Int. Ed.* **2020**, *59*, 19434.

[24] S. Liang, M. Zhang, G. M. Biesold, W. Choi, Y. He, Z. Li, D. Shen, Z. Lin, *Adv. Mater.* **2021**, *33*, 2005888.

[25] J. Pan, Y. Shang, J. Yin, M. De Bastiani, W. Peng, I. Dursun, L. Sinatra, A. M. El-Zohry, M. N. Hedhili, A. H. Emwas, O. F. Mohammed, Z. Ning, O. M. Bakr, *J. Am. Chem. Soc.* **2018**, *140*, 562.

[26] H. Li, H. Lin, D. Ouyang, C. Yao, C. Li, J. Sun, Y. Song, Y. Wang, Y. Yan, Y. Wang, Q. Dong, W. C. H. Choy, *Adv. Mater.* **2021**, *33*, 2008820.

[27] F. Krieg, Q. K. Ong, M. Burian, G. Raino, D. Naumenko, H. Amenitsch, A. Suess, M. J. Grotevent, F. Krumeich, M. I. Bodnarchuk, I. Shorubalko, F. Stellacci, M. V. Kovalenko, *J. Am. Chem. Soc.* **2019**, *141*, 19839.

[28] Y. He, Y. Liang, S. Liang, Y. W. Harn, Z. Li, M. Zhang, D. Shen, Z. Li, Y. Yan, X. Pang, Z. Lin, *Angew. Chem., Int. Ed.* **2021**, *60*, 7259.

[29] Y. J. Yoon, Y. Chang, S. Zhang, M. Zhang, S. Pan, Y. He, C. H. Lin, S. Yu, Y. Chen, Z. Wang, Y. Ding, J. Jung, N. Thadhani, V. V. Tsukruk, Z. Kang, Z. Lin, *Adv. Mater.* **2019**, *31*, 1901602.

[30] C. Murray, D. J. Norris, M. G. Bawendi, *J. Am. Chem. Soc.* **1993**, *115*, 8706.

[31] J. Shi, F. Li, Y. Jin, C. Liu, B. Cohen-Kleinstein, S. Yuan, Y. Li, Z. K. Wang, J. Yuan, W. Ma, *Angew. Chem., Int. Ed.* **2020**, *59*, 22230.

[32] S. Wang, L. Du, Z. Jin, Y. Xin, H. Mattoussi, *J. Am. Chem. Soc.* **2020**, *142*, 12669.

[33] H. Kim, N. Hight-Huf, J. H. Kang, P. Bisnoff, S. Sundararajan, T. Thompson, M. Barnes, R. C. Hayward, T. Emrick, *Angew. Chem., Int. Ed.* **2020**, *59*, 10802.

[34] B. A. Koscher, J. K. Swabeck, N. D. Bronstein, A. P. Alivisatos, *J. Am. Chem. Soc.* **2017**, *139*, 6566.

[35] S.-m. Chang, P.-h. Lo, C.-t. Chang, *Appl. Catal., B* **2009**, *91*, 619.

[36] R. Tantipolphan, T. Rades, A. J. McQuillan, N. J. Medlicott, *Int. J. Pharm.* **2007**, *337*, 40.

[37] T. Y. Ma, S. Z. Qiao, *ACS Catal.* **2014**, *4*, 3847.

[38] Z. Chu, Q. Ye, Y. Zhao, F. Ma, Z. Yin, X. Zhang, J. You, *Adv. Mater.* **2021**, *33*, 2007169.

[39] H. Zhou, J. Park, Y. Lee, J. M. Park, J. H. Kim, J. S. Kim, H. D. Lee, S. H. Jo, X. Cai, L. Li, X. Sheng, H. J. Yun, J. W. Park, J. Y. Sun, T. W. Lee, *Adv. Mater.* **2020**, *32*, 2001989.

[40] S. Yuan, Z.-K. Wang, M.-P. Zhuo, Q.-S. Tian, Y. Jin, L.-S. Liao, *ACS Nano* **2018**, *12*, 9541.

[41] P. Teng, S. Reichert, W. Xu, S.-C. Yang, F. Fu, Y. Zou, C. Yin, C. Bao, M. Karlsson, X. Liu, J. Qin, T. Yu, W. Tress, Y. Yang, B. Sun, C. Deibel, F. Gao, *Matter* **2021**, *4*, 3710.

[42] R. Brenes, C. Eames, V. Bulovic, M. S. Islam, S. D. Stranks, *Adv. Mater.* **2018**, *30*, 1706208.

[43] D. Han, M. Imran, M. Zhang, S. Chang, X. G. Wu, X. Zhang, J. Tang, M. Wang, S. Ali, X. Li, G. Yu, J. Han, L. Wang, B. Zou, H. Zhong, *ACS Nano* **2018**, *12*, 8808.

[44] J. Jang, Y. H. Kim, S. Park, D. Yoo, H. Cho, J. Jang, H. B. Jeong, H. Lee, J. M. Yuk, C. B. Park, D. Y. Jeon, Y. H. Kim, B. S. Bae, T. W. Lee, *Adv. Mater.* **2021**, *33*, 2005255.

[45] F. Bickelhaupt, E. Baerends, C. F. Guerra, S. Van Gisbergen, J. Snijders, T. Ziegler, *J. Comput. Chem.* **2001**, *22*, 931.

[46] J. Liu, K. Song, Y. Shin, X. Liu, J. Chen, K. X. Yao, J. Pan, C. Yang, J. Yin, L.-J. Xu, *Chem. Mater.* **2019**, *31*, 6642.